Brazilian Journal
of Chemical
Engineering

ISSN 0104-6632
Printed in Brazil
www.abeq.org.br/bjche

Vol. 36, No. 03, pp. 1175 - 1184, July - September, 2019
dx.doi.org/10.1590/0104-6632.20190363s20190023

CATALYTIC OXIDATION OF ISOPROPYL ALCOHOL OVER PLATINUM BASED CATALYST: A STUDY OF THE EFFECT OF METHYL CELLULOSE ON Pt PARTICLES DISPERSION OVER MULLITE

R. Abbas-Ghaleb[1,2*] and D. Chlala[1,2,3]

[1] Lebanese University, Faculty of Engineering, Laboratory of Chemical Engineering, Roumieh, Lebanon.
E-mail: reine.ghaleb@ul.edu.lb - ORCID: 0000-0002-0897-8498; ORCID: 0000-0002-9830-3389
[2] Lebanese University, Doctoral School for Science and Technology, Platform for Research in NanoSciences and NanoTechnology, Fanar, Lebanon.
[3] Lebanese University, Faculty of Sciences, Laboratory of Physical Chemistry of Materials, Jdeidet El Metn, Lebanon.

(Submitted: January 20, 2019 ; Revised: March 15, 2019 ; Accepted: March 27, 2019)

Abstract - Isopropyl alcohol (IPA) catalytic oxidation remains one of the most popular techniques to remove volatile organic compounds from indoor places. In our study, catalytic oxidation of IPA was investigated on catalysts based on platinum deposited on mullite ($Al_6Si_2O_{13}$), known for its excellent thermal stability. Pt/$Al_6Si_2O_{13}$ catalysts were prepared by impregnation with and without methyl cellulose (MC) and were tested in order to study the influence of MC on the platinum particle dispersion over the support. The catalytic reactivity was compared with Pt/α-alumina and Pt/SiO_2. Moreover, the resulting materials were characterized by BET, XRD, TEM and H_2-chemisorption. This study showed that platinum exhibits better dispersion on alumina sites than silica sites. This can be due to a strong interaction between platinum and alumina, leading to a higher dispersion of platinum species. Furthermore, the addition of MC enhanced the Pt dispersion over the mullite, leading to an improvement in the catalytic performance.
Keywords: VOCs; Isopropyl alcohol; Platinum; Methyl cellulose; Mullite; Fragrance lamps.

INTRODUCTION

Volatile organic compounds (VOCs), which are emitted by various industrial processes such as petroleum refineries, fuel combustion and chemical industries, are considered as the first source of outdoor and indoor environmental pollutants in living and working places (Berenjian et al., 2012). Indoor sources include solvents used in the production and maintenance of building materials, furnishings or equipment such as paint.

Among the different techniques available for VOCs abatement, flameless catalytic fragrance lamps that auto-catalytically burn an alcohol-fragrance mixture remain one of the techniques to treat these harmful pollutants (Berenjian et al., 2012; Khan and Ghoshal., 2000). This latter is usually based on the total catalytic oxidation of isopropyl alcohol (IPA), which is a highly flammable liquid, in air into CO_2 and water. Such technologies are used in the fragrance lamp industry to remove indoor environmental pollutants.

In fact, isopropyl alcohol, with a high vapor pressure of 42.74 mm Hg at 25 °C, is used as a carrier for the fragrance. The alcohol-fragrance mixture, composed of approximately 90% of IPA and 10% of fragrance, is transported from a reservoir to a flameless catalytic burner, which simultaneously combusts the alcohol while dispersing the fragrance in the surrounding atmosphere. Their high vapor pressure allows them to soak the wick, which transports them to the burner. The catalytic oxidation of IPA can be carried out at

* Corresponding author: R. Abbas-Ghaleb - E-mail: reine.ghaleb@ul.edu.lb

temperatures 300–500 °C lower than that required for thermal oxidation (Berenjian et al., 2012).

Catalysts used for this application may contain various metal oxides such as chromium oxide or nickel oxide, in addition to other noble metals such as Pt, Pd and Rh (Berenjian et al., 2012; Yee et al.,2000; Spivey, 1987). Supported gold nanoparticles are applied for low temperature combustion of VOC (Liotta, 2010; Ousmane et al., 2011). Thus, precious metals supported on metal oxide catalysts are used for low-temperature combustion of VOC and more specifically Pt/α-Al_2O_3 or Pt/SnO_2 (Leclerq et al., 2014). In addition, different forms of zeolite based burners such as ZSM-5 were also used. The surface area of catalysts already used ranges from 10 m^2/g to 1000 m^2/g (Balkus and Pisklak, 2011).

Furthermore, it was found that the catalytic activity, selectivity and stability of the metal-based oxides depend on several parameters such as: the metal particle size and their dispersion, the type of support, the preparation method, the calcination temperature and the pretreatment procedure (Aboukais et al., 2016). Moreover, increasing the metal particle dispersion may help in decreasing the amount of the metallic phase on the surface and reducing the catalyst cost. Thus, increasing the efficiency and the selectivity of the catalyst can be beneficial for the fragrance lamp industry.

Previous studies on Pt deposited on silicon carbide (SiC), revealed that the catalyst performance depends on the amount of Pt used and its dispersion on the surface (Liu et al., 2017). On the other hand, Nguyen et al. (2007) reported that the addition of glycerol into the catalyst preparation can enhance metal particle dispersion. Furthermore, it has been reported that methyl cellulose (MC), one of the simplest cellulose derivatives, has an excellent film and emulsion forming ability with TiO_2, SiO_2 and some metal ions (Kamitakahara et al., 2008; Chen et al., 2005). Moreover, MC has been previously used in many catalyst preparations such as synthesis of zeolite and silver particles (Rangelova et al., 2011).

Mullite is an aluminosilicate compound and a characteristic constituent of all ceramic products. It has been used as a refractory for millennia and it is commonly denoted $3Al_2O_3.2SiO_2$ or $Al_6Si_2O_{13}$. Mullite is one of the important constituents of porcelain known for properties such as: good thermal shock resistance, good high temperature strength, excellent thermal stability, resistance to oxidation and attack by furnace atmospheres, resistance to abrasion, superior corrosion resistance to most chemicals and good electrical resistivity (Schneider et al., 2008). All these properties made mullite a good candidate to be used in the lamp industry. New uses are being found for this material in the areas of electronics and optics as well as in high temperature structural products (Mizuno, 1991).

In catalysis, Mullite was reported in different applications such as catalytic combustors for the reverse water gas shift reaction on Pt/mullite (Liang et al., 2017). Also, it was previously used in catalytic craking units (FCC) for promoting the combustion of carbon monoxide to carbon dioxide and in the wet peroxide oxidation of phenol (Corma and Mocholi, 1992). In addition, Wang et al. (2012) reported a mullite catalyst with remarkable catalytic performance towards NO oxidation. Furthermore, Mn-mullite replaced the platinum in the catalytic oxidation of diesel soot (Wang et al., 2012).

For this specific catalyst, octahedral and pyramidal crystal fields coexist, so that this structure has partial characteristics of both zeolithes and common oxides like Al_2O_3 and SiO_2 (Xue et al., 2017).

To the best of our knowledge, no reports in the literature deal with IPA catalytic oxidation over platinum supported on mullite. Thus, the aim of this work is to: (i) optimize Pt particle dispersion over mullite with a low surface area by adding MC to the impregnation procedure; (ii) evaluate the catalytic performances of the obtained solids towards reaching a total oxidation of IPA into CO_2 and H_2O; and (iii) compare its catalytic performances with other catalysts such as Pt/α-Al_2O_3 and Pt/SiO_2.

MATERIALS AND METHODS

Catalysts preparation

The conventional wet impregnation method, which is the simplest, easiest and least expensive method, was used to prepare Pt/Mullite catalysts without or with Methyl Cellulose.

Preparation of 0.6wt% Pt/$Al_6Si_2O_{13}$ without Methyl Cellulose

The Mullite support used in our experiments was purchased from Tritrust Industrial Co (China) with a surface area of 12 m^2/g. An adequate amount of tetraammine platinum (II) chloride, $(NH_3)_4PtCl_2.H_2O$ (Sigma Aldrich, purity 98 %), precursor was dissolved in excess distilled water before adding the required amount of Mullite support. The slurry was stirred for 1 h at 60 °C, in a rotary evaporator. Water was then removed under reduced pressure and the obtained solid was dried for about 24 h in an oven at 110 °C. The catalyst was treated at 500 °C under N_2 for 30 min then reduced under H_2 for 2 h and retreated under N_2 for 30 min in order to allow hydrogen removal. This solid is denoted Pt/$Al_6Si_2O_{13}$ in which the Pt content was 0.6 wt%.

Pt species were also impregnated on SiO_2 and α-Al_2O_3 supports for comparison purposes using the same experimental procedure described for Pt/$Al_6Si_2O_{13}$ with Pt content of 0.6 wt%. The reference

silica support was prepared by calcination of β-SiC supplied by Sigma-Aldrich (purity 97.5 %; surface area = 36 $m^2.g^{-1}$) at 1100 ºC for 5 h under air. As for the reference alumina support, it was supplied by SCS9 (α) Rhône-Poulenc (purity 99.9 %; surface area = 8 $m^2.g^{-1}$) and used as received. The as-prepared catalysts will be designed hereafter by Pt/SiO_2 and $Pt/\alpha\text{-}Al_2O_3$.

Preparation of 0.6wt% $Pt/Al_6Si_2O_{13}$ with Methyl Cellulose (MC)

Pure methyl cellulose (MC) obtained from Sigma-Aldrich (purity 31.5 %) was used as an additive to form a hydrogel. Following the same procedure, the adequate amount of MC and tetraammine platinum (II) chloride was mixed in water to give the desired MC and Pt loading (2.1 wt% and 6.4 wt% respectively). The formed gel was used as a precursor to obtain the new catalyst designated as $Pt/Al_6Si_2O_{13}$(MC) using the same procedure described for $Pt/Al_6Si_2O_{13}$.

Characterization of the catalysts

The quantification of the Pt content was performed on the reduced solids, using inductively coupled plasma - atomic emission spectroscopy (ICP-AES) on an Activa-Horiba (Jobin Yvon S.A.S) spectrometer. Analysis was carried out at the Claude Bernard University Lyon I. Prior to analysis, the solids were treated by a mixture of concentrated hydrochloric and nitric acids (70 %-30 %). Phase determination was performed using X-ray diffraction (XRD) at ambient temperature of the reduced solids. The X-ray diffractograms were recovered with a SIEMENS D500 ® diffractometer using Cu $K_{\alpha 1}$ radiation (λ=1.5406 Å Ni filtered). Diffraction data were recovered from 10° to 80 in 2θ angles with a step of 0.02° and a count time of 16 s. The XRD patterns were indexed by comparison with PDFs. The crystallite size of Pt [thickness of crystal in a direction perpendicular to the (111) lattice plan] was determined by TOPAS software using the following Scherrer's equation:

$$C_S = \frac{K\lambda}{\beta \cos\theta} \quad (1)$$

where β is a half width, λ is wavelength (0.154 nm), θ is Bragg angle (2θ = 39.7°) and K is the Scherrer's constant of 0.9.

The specific surface areas of the materials were measured by using the physisorption technique at 77 K. The experiences were performed in Micromeritics ASAP 2020 equipment. Before starting the analysis, the samples were outgassed under vacuum at 300 °C for 2 h. Particle dispersion was determined by H_2 Chemisorption after reducing the catalyst in pure hydrogen flow for 2 h at 300 °C. The quantitative determination of chemisorbed hydrogen by temperature programmed desorption (TPD) was used as a standard method to characterize the dispersion state of supported platinum.

Before carrying out the chemisorption, the sample (approximately 400 mg) is treated under air at 300 °C for 1 h and then reduced in a dilute hydrogen solution in argon (1%vol H_2, Ar) from 25 °C to 300 °C (10 °C.min^{-1}) with a stand-by at 300 °C for 2 h. In order to remove all traces of hydrogen, the sample was purged under argon at 300 °C for 1 h and then cooled under an argon flow to ambient temperature at which the chemisorptions of hydrogen was performed. The measurement was carried out by passing a series of hydrogen pulses (5) into the sample at a regular interval of time. This non-adsorbed amount is null at the beginning because all the hydrogen is adsorbed and then it increases with the pulses until becoming constant (saturation). The difference between the amount of unadsorbed gas and the amount of hydrogen sent will give the amount of gas adsorbed for each pulse. In order to measure the H_2 content in argon, a microcatharometer connected with a signal amplifier was used. The amount of unadsorbed gas was detected by the apparatus. The morphology of the prepared solids was examined at room temperature using a JEOL 100 CX ® TEM operating at an accelerating voltage of 100 kV and equipped with energy dispersive X-ray spectroscopy (EDAX). Prior to TEM observations, samples were deposited from ethanolic solution onto porous-carbon copper grids.

Catalytic performance test

The isopropyl alcohol catalytic oxidation experiments were performed under atmospheric pressure. For each catalytic run, about 20 mg of catalyst was placed in the continuous-flow fixed-bed Quartz reactor located in an electrical furnace. The concentration of isopropyl alcohol was controlled by the temperature of the saturator (20 °C) placed in a dewar flask (P_{IPA} = 32 Torr) and the additional air stream. The flow rate of the reactive gas mixture through the reactor was 167 mL/min and consisted of IPA (5 vol%) and air (95 vol%), which correspond to a Volume Hourly Space Velocity (VHSV) of 500 $m^3.kg^{-1}.h^{-1}$.

Before each run, the samples were pretreated for 1 h at 300 °C under H_2 flow of 30 mL/min and 30 min under N_2 flow of 33 mL/min. Catalyst performances were evaluated in a temperature range of 50 -550 °C with an increasing rate of 1°C/min.

The IPA inlet and outlet concentrations were analyzed using a Chromatopac Shimadzu Gas Chromatograph (GC-14A) equipped with a flame ionization detector connected to a PoraBOND Q column. As for CO_2, its concentration was analyzed with a catharometer detector connected to a Porapak Q column.

Isopropyl alcohol conversion (C_t) was calculated as follows:

$$C_t\,(\%) = 100 \times \frac{[IPA]_i - [IPA]_t}{[IPA]_i} \quad (2)$$

where $[IPA]_i$ and $[IPA]_t$ represent respectively IPA inlet and outlet concentrations.

The selectivity towards CO_2 (S_{CO2}) was determined by:

$$S_{CO_2}\,(\%) = 100 \times \frac{[CO_2]t/3}{[IPA]_i - [IPA]_t} \quad (3)$$

where $[CO_2]_t$ is the CO_2 outlet concentration.

The turnover frequency TOF (the number of molecules converted per catalytic active site per time) was calculated by using the following formula:

$$TOF\left(s^{-1}\right) = \frac{C_{(t)} \times F \times M_{Pt}}{m_{cat} \times X_{Pt} \times D_{Pt}} \quad (4)$$

where $C_{(t)}$ is the IPA conversion (%), F the initial molar flow rate of IPA (mol.s^{-1}), M_{Pt} the molar weight of Pt (195.08 g.mol^{-1}), m_{cat} the amount of catalyst (g), X_{Pt} the Pt content determined by ICP-AES and D_{Pt} the dispersion of Pt.

RESULTS AND DISCUSSION

Catalyst characterization

Chemical composition value, BET surface area, platinum dispersion obtained by H_2 chemisorption, crystallite size calculated using Scherrer's equation and revealed by TEM are shown in Table 1.

The ICP results indicate that the Pt content was very close to that expected for the impregnated samples. The specific surface areas of Pt deposited on mullite prepared with or without MC were 6 m^2/g indicating that the addition of methyl cellulose has no influence on the specific surface area. As for Pt/α-Al_2O_3 and Pt/SiO_2, the specific surface areas were 8 m^2/g and 18 m^2/g respectively.

The X-ray diffractograms obtained at room temperature for the different solids are depicted in Fig.1. The α-Al_2O_3 phase (JCPDS card No.10-0173) with space group R-3c (X-ray diffraction peaks marked by • in Fig. 1) was detected. The mullite sample and both Pt/mullite samples with or without MC present 19 diffraction peaks marked with ◊ in Fig. 1 that correspond to the orthorhombic phase $Al_6Si_2O_{13}$ (JCPDS No. 15-0776), known as mullite with the space group Pbam (Agathopoulos et al., 2004; Shackelfork and Doremus, 2008). Also, we noticed the presence of other diffraction peaks at 2θ = 25.6°, 37.8°, 43.4°, 57.6°, 77.3° and 77.78° that correspond to the α-Al_2O_3 phase (Sedaghat et al., 2013). Moreover, the X-ray diffraction pattern of mullite and Pt/$Al_6Si_2O_{13}$ displays new peaks positioned at 2θ = 35°, 60° and 72°. These peaks revealed the presence of impurities that already exist in the mullite used in this study (Dhiman et al., 2013; Ledoux and Pham-Huu, 2001; Orrego-Romero et al., 2016).

Moreover, the presence of reduced platinum in all the samples was confirmed by the observation of two diffraction peaks assigned to Pt crystal planes (111) and (200), corresponding to 39.7° and 46.2°, respectively (JCPDS 65-2868) (Dhiman et al., 2013).

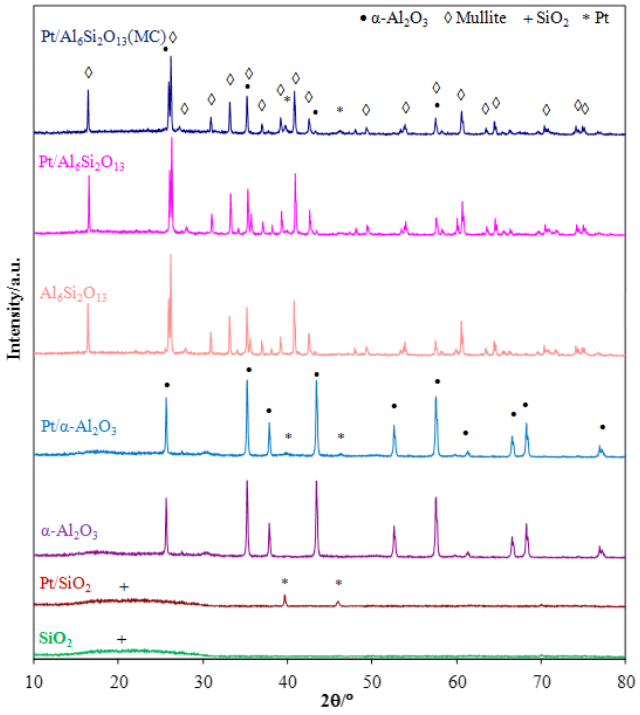

Figure 1. X-ray diffraction of the supports before and after the addition of Pt.

Table 1. Chemical composition, Pt dispersion and crystallite size of the samples.

Sample	Pt (wt%)	Surface area (m^2/g)	Pt dispersion (%)	Crystallite size Scherrer (nm)	TEM Pt particle size (nm)
Pt/$Al_6Si_2O_{13}$	0.58	6	22	50	5 nm (few particles of 10-50 nm)
Pt/$Al_6Si_2O_{13}$(MC)	0.6	6	36	18	1-5 nm (few particles of 10-20 nm
Pt/α-Al_2O_3	0.58	8	56	48	2 nm (few particles of 50nm)
Pt/SiO_2	0.6	18	6	75	20-100 nm

Also, the impregnation of Pt on all the supports does not affect their structure as the position and intensity of its diffraction peaks do not change significantly with the addition of Pt, and no loss of crystallinity is observed. Platinum crystallite sizes illustrated in Table 1 were estimated by XRD pattern based on using Scherrer's equation for the peak at 2θ =39.7° on Pt/α-Al_2O_3 and Pt/SiO_2. The calculated Pt crystallite size values were 48 nm and 75 nm on Pt/α-Al_2O_3 and Pt/SiO_2 respectively. On the other hand, platinum crystallite size was equal to 50 nm for Pt/$Al_6Si_2O_{13}$. After the addition of MC, this value decreases to 18 nm for the Pt/$Al_6Si_2O_{13}$(MC) sample.

The dispersion of platinum particles for Pt/α-Al_2O_3 and Pt/SiO_2 obtained by the H_2 chemisorption method, given as an average value, was respectively 56% and 6%. For Pt/$Al_6Si_2O_{13}$, platinum dispersion was equal to 22%. A higher dispersion of 36% was observed for the Pt catalyst prepared with MC.

In order to gain more insight on the textural properties of the samples and to better understand such results, transmission electron microscopy (TEM) was performed for the catalysts. A TEM image and the summary of energy dispersive X-ray analysis (EDAX) results for the mullite sample are represented respectively in Fig. 2 and Table 2.

The TEM image shows 3 distinctive zones corresponding to Al_2O_3 (alumina), SiO_2 (quatz) and $Al_6Si_2O_{13}$ (mullite) with a ratio Al/Si ≈ 2-3. Energy Dispersive X-Ray Analysis (EDAX) was also used to identify the elemental composition of the mullite and in order to run structural analysis. This analysis confirmed the presence of O, Al, and Si elements and indicated the presence of impurities in the mullite.

Table 2. Summary of EDAX results on the mullite sample.

Element	Atomic composition (%)
O	56.64
Al	28.19
Si	15.17

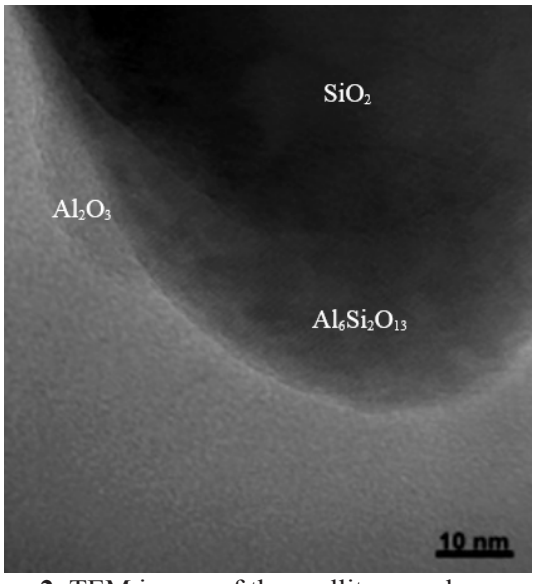

Figure 2. TEM image of the mullite sample.

Representative TEM images of the Pt supported catalysts are illustrated in Fig. 3 and 4. The TEM images show the size of the platinum particles dispersed on the different supports.

It is noted that for Pt/α-Al_2O_3 the average particle size in TEM images was about 2 nm with the presence of a few other particles with a higher diameter of 50 nm (Fig.3a and Fig.3b). These particles with a high diameter of 50 nm are possibly the same particles previously detected by XRD since it is difficult to detect by X-ray diffraction small platinum particles at low concentration (Nagai et al., 2011). TEM results

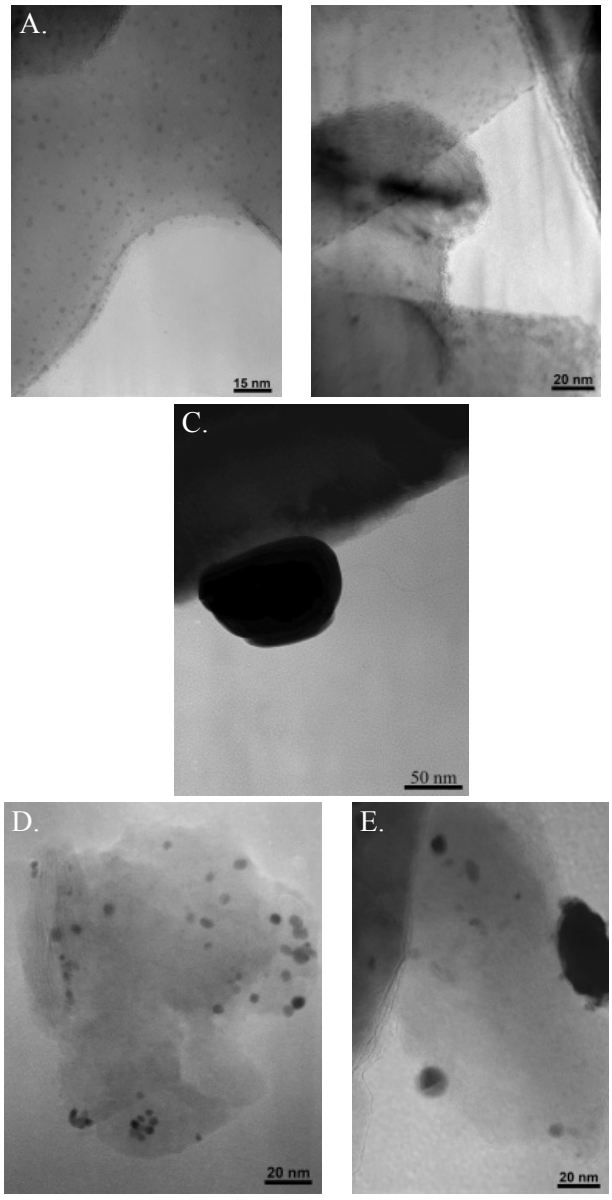

Figure 3. TEM images of a,b: Pt/α-Al_2O_3; c: Pt/SiO_2; and d,e: Pt/$Al_6Si_2O_{13}$.

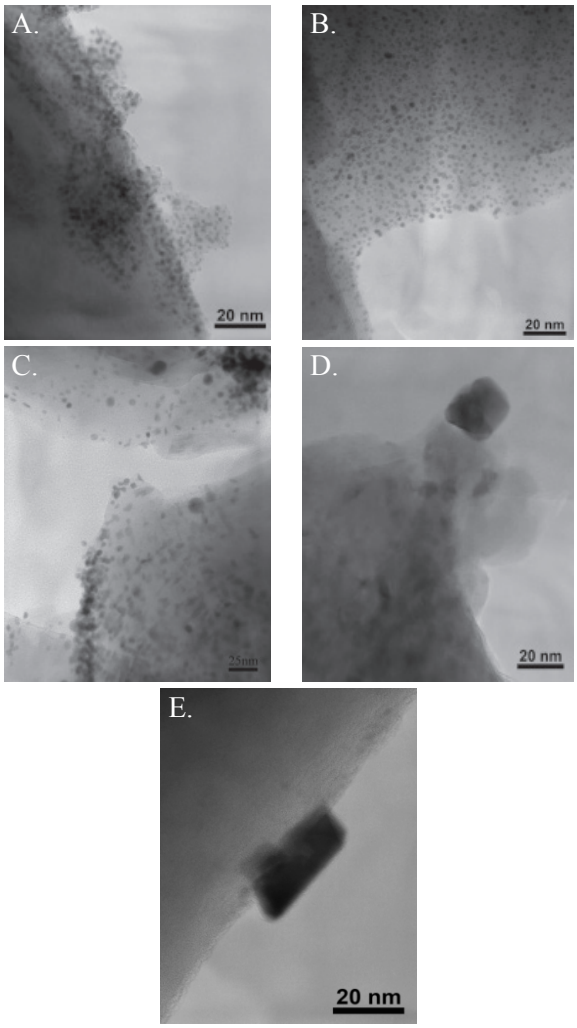

Figure 4. TEM images of $Pt/Al_6Si_2O_{13}$(MC).

showed well distributed species, in agreement with the result obtained with the H_2 chemisorption method (56%).

In addition, for the SiO_2 sample the TEM image showed that the particle size ranged from 20 to 100 nm (Fig.3c). Furthermore, for $Pt/Al_6Si_2O_{13}$, Pt species are illustrated in Fig.3d and e and the particle sizes were around 5 nm in addition to a few particles of size between 10-50 nm. Pt particles were not well dispersed on mullite with the presence of platinum free areas; in fact, Pt species are located in the same region where Al is present.

However, after the addition of methyl cellulose to the synthesis of Pt deposited on mullite (Fig.4), TEM images showed that Pt particle size varied between 1 nm and 5 nm with an improvement in the Pt dispersion (Fig.4a,b and c). In addition, it is noteworthy to mention the presence of a few particles with a diameter range between 10 and 20 nm (Fig.4d and e). These particles are possibly the same particles previously detected by XRD according to Scherrer's equation. Therefore, these results indicate that the addition of MC enhanced the Pt dispersion on the mullite support. Such a result is in agreement with the dispersion values obtained by the H_2 chemisorption method and crystallite size estimated by XRD.

Also, platinum particle size distributions (%) via particles size (nm) were estimated from statistical counting of platinum particles. Particle size distributions are represented in Figs 5 and 6.

Particle size distributions were determined via transmission electron microscopy (TEM). We observed an heterogeneous particle size distribution since Pt particles were not uniformly distributed on the different supports. For $Pt/\gamma\text{-}Al_2O_3$, the particle size distribution (PSD) indicates smaller platinum particles. The major particle size is approximately 2 nm with the presence of a minority of particles of size 48 nm. On Pt/SiO_2 a bigger major particle size of 75 nm with a few particles of 20 and 50 nm were detected. On the other hand, the PSD indicates particles on $Pt/Al_6Si_2O_{13}$ with a major size of 5 nm with a few particles of 10 and 46 nm and on $Pt/Al_6Si_2O_{13}$(MC) a major particle size of 2 nm with the presence of a few particles of 10 to 20 nm. This result is in agreement with the dispersion values obtained by the H_2 chemisorption method and crystallite size estimated by XRD for platinum particles with high diameter.

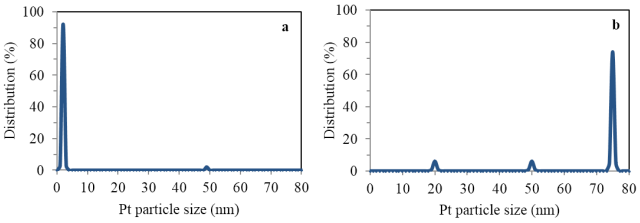

Figure 5. Particle size distributions (a- Pt/Al_2O_3 ; b- Pt/SiO_2).

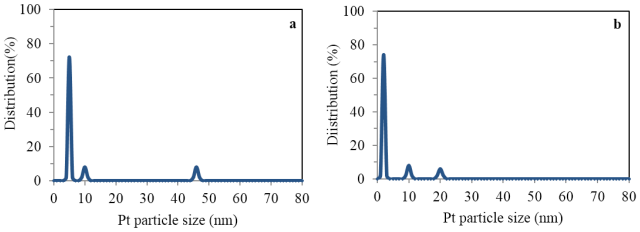

Figure 6. Particle size distributions (a- $Pt/Al_6Si_2O_{13}$; b- $Pt/Al_6Si_2O_{13}$ (MC)).

Catalytic activity

In order to evaluate the performance of the catalysts in IPA oxidation, the IPA conversion as a function of temperature over Pt supported catalysts is given in Fig. 7. The T_{10}, T_{50} and T_{90} values, the temperatures at which respectively 10, 50 and 90% of IPA is converted, were extracted from these light-off curves and are listed in Table 3.

The oxidation of isopropyl alcohol regarding the catalyst used starts around 100°C (Fig.7). The complete oxidation of IPA is achieved for $Pt/\alpha\text{-}Al_2O_3$

and Pt/mullite(MC) catalysts at 350 ºC, while at this temperature the conversion is 90 % for the Pt/mullite sample. Thus the MC addition enhanced the IPA conversion on the mullite support. However, for the Pt/SiO_2 catalyst, only 80 % of IPA were converted at 500 ºC.

The IPA conversion based on T_{50}(ºC) decreases as follow: $Pt/\alpha\text{-}Al_2O_3$(164ºC) ≈ $Pt/Al_6Si_2O_{13}$(MC) (168 ºC) $Pt/Al_6Si_2O_{13}$ (179 ºC) > Pt/SiO_2 (232ºC).

In order to check the real activity for the different catalysts, the turnover frequency (TOF) was determined at low IPA conversion (approximately ≈ 10%) from the number of surface Pt atoms (Briand et al., 2003). The TOF was therefore calculated at 120°C for the different catalysts. The TOF values are presented in Table 3. This table reveals that the TOF value for $Pt/Al_6Si_2O_{13}$ (MC) was 0.047 s^{-1}, very similar to that found for $Pt/\alpha\text{-}Al_2O_3$ (0.045 s^{-1}). This behavior is in agreement with the IPA oxidation conversion presented above for the different catalytic systems. The results clearly show that the catalytic activity of $Pt/Al_6Si_2O_{13}$(MC) is similar to that found for Pt/Al_2O_3. Furthermore, the TOF value obtained for $Pt/Al_6Si_2O_{13}$ (MC) is higher than the TOF value obtained for $Pt/Al_6Si_2O_{13}$ (0.025 s^{-1}). It seems that the nature of the surface active sites for Pt deposited on $Al_6Si_2O_{13}$ after the addition of methylcellulose (MC) is more efficient than the platinum active sites for $Pt/Al_6Si_2O_{13}$ without MC. This result indicate that the addition of MC improved the catalyst activity.

In order to understand more the catalyst performance, the CO_2 selectivity as a function of temperature is illustrated in Fig. 8. It is noteworthy to mention that the temperature at which the CO_2 formation arises are shifted to 150 °C for $Pt/\alpha\text{-}Al_2O_3$ and $Pt/Al_6Si_2O_{13}$(MC) and to 200 °C for $Pt/Al_6Si_2O_{13}$ and Pt/SiO_2. According to many authors, this shift could be explained by the formation of acetone at low temperatures (Centeno et al., 2002; Scirè et al., 2003; Tu et al., 2012). In addition, 100 % of CO_2 selectivity can be reached at approximately 500 °C for $Pt/\alpha\text{-}Al_2O_3$ and $Pt/Al_6Si_2O_{13}$(MC). Otherwise, such selectivity cannot be reached on $Pt/Al_6Si_2O_{13}$ and Pt/SiO_2. In fact, CO_2 selectivity for $Pt/Al_6Si_2O_{13}$ and Pt/SiO_2 at 550 °C is around 80 % and 70 % respectively. This can be explained by the formation of other products (ketones) since the IPA oxidation reaction was not complete (Centeno et al., 2002; Scirè et al., 2003).

This result can be explained by the fact that MC is a dispersing agent that inhibits the agglomeration of active components, controls the particle size and distribution, and also influences the surface morphology (Liu et al., 2017; Rangelova et al., 2011). It seems that MC played an important role during the impregnation process of supported metal. In fact, the addition of MC increases the viscosity upon solution evaporation, which inhibited redistribution of the Pt particles. Furthermore, the enhanced viscosity due to MC can inhibit the migration of impregnation solutions to the external edge of the support bodies during the drying process, which contributes to the uniform distribution

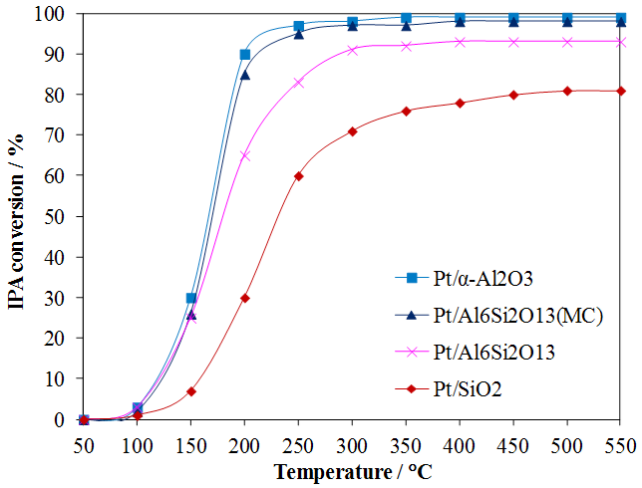

Figure 7. Conversion of isopropanol alcohol on different catalysts **.**

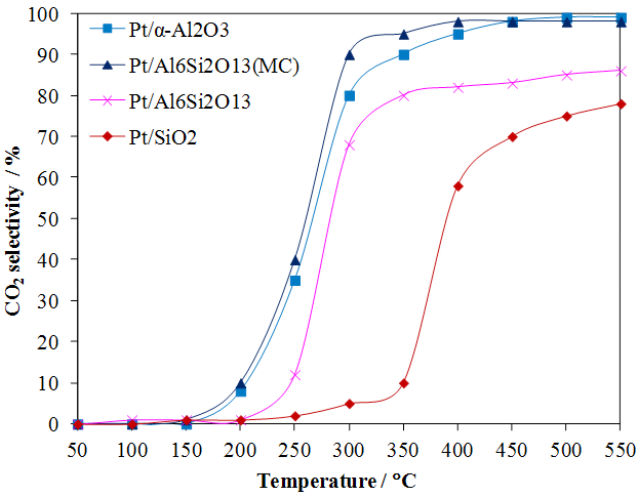

Figure 8. CO_2 selectivity on the different catalysts.

Table 3. Temperatures at 10 %, 50 % and 90 % IPA conversions, respectively T_{10}, T_{50} and T_{90} (ºC), and the turnover frequencies at 120 ºC (low IPA conversion) for the different studied catalysts.

Catalyst	Dispersion (%)	T_{10} (ºC)	T_{50} (ºC)	T_{90} (ºC)	TOF (s^{-1}) at 120°C
$Pt/\alpha\text{-}Al_2O_3$	56	120	164	200	0.045
$Pt/Al_6Si_2O_{13}$(MC)	36	120	168	215	0.047
$Pt/Al_6Si_2O_{13}$	22	120	179	300	0.025
Pt/SiO_2	6	160	232	-	0.013

of the active phase over the support and avoids the agglomeration of metal precursor and favors a high dispersion of active component (Liu et al., 2017). Therefore, inhibiting the loss of active phase may favor the catalyst activity and stability (Brackmann at al., 2014). This explanation can be illustrated in Fig.9.

Pesant et al. (2004) reported a strong interaction between Pt species and alumina. According to their TEM results, no Pt particles were seen to exist alone on the support SiO_2. Platinum was far away from Si species of the support. Pt species were located in the same region where Al was present. Dai et al. (2017) also showed in their studies that the cellulose content has little effect on the pore size distribution but it is known as an excellent dispersing agent and this can explain the non change in the surface specific area for $Pt/Al_6Si_2O_{13}$ with and without MC but only on the platinum particle dispersion.

Thus, platinum species could be localized on specific areas which could be attributed to aluminum sites since TEM images showed that Pt particles exhibit better dispersion on aluminum sites (Fig.3a) than on the silica ones (Fig.3c). This difference is due to a possible interaction between Pt and Al. Besides, the weak interaction between silica sites and the Pt species was previously reported by Pesant et al. (2004). These interactions seem to be less efficient, resulting in a lower dispersion of platinum supported on β-SiC. Furthermore, the presence of MC was effective in improving the catalytic behavior of the catalyst which is due to the increase in the Pt particle dispersion already observed in TEM and obtained by H_2 chemisorption. The increase in the activity for $Pt/Al_6Si_2O_{13}$(MC) compared with $Pt/Al_6Si_2O_{13}$ is related to the higher dispersion of platinum already obtained by using methyl cellulose as a dispersing agent during the synthesis by wet impregnation. In fact, the improvement in the particle dispersion leads to a higher number of catalytic active sites deposited on the support upon interaction (Xingneng et al., 2012). This result correlates as well with our hypothesis about a possible interaction between Pt and alumina sites that increase on mullite with the addition of MC.

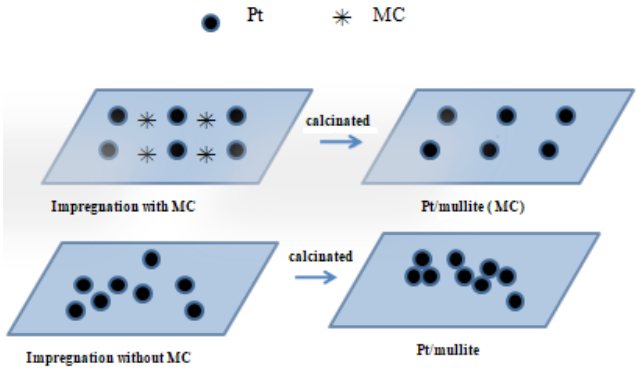

Figure 9. Schematic illustration of effect of MC on Pt particles dispersion.

CONCLUSIONS

This study sheds light on the effect of adding MC to the catalyst preparation method in order to improve the Pt dispersion on the support. Transmission electron microscopic measurements showed that the Pt nanoparticles were better dispersed on the mullite in the presence of methyl cellulose. The resulting Pt nanoparticles exhibited better activity towards isopropyl alcohol oxidation with the best performance among the series of samples. The results of this study show that methyl cellulose presents attractive advantages for the application in fragrance lamp industries.

ACKNOWLEDGMENTS

The authors sincerely acknowledge the Claude Bernard University Lyon I (France) for performing the TEM images and the ICP-AES analysis.

REFERENCES

Aboukais, A., Skaf, M., Hany, S., Cousin, R., Aouad, S., Labaki, M., Abi-Aad, E. A comparative study of Cu, Ag and Au doped CeO2 in the total oxidation of volatile organic compounds (VOCs). Material Chemistry and Physics, 177, 570-576 (2016). https://doi.org/10.1016/j.matchemphys.2016.04.072

Agathopoulos, S., Fernandes, H.R., Tulyaganov, D., Ferreira, J.M.F. Preparation of mullite whiskers from kaolinite using $CuSO_4$ as fluxing agent. Materials Science Forum, 455-456, 818-821 (2004). https://doi.org/10.4028/www.scientific.net/MSF.455-456.818

Balkus, K.J., Pisklak, T.J. Vapor pressure fuels for use in aromatherapy and fragrance lamps. U.S. Patent N°. 8,062,389(2011).

Berenjian, A., Chan, N., Jafarizadeh Malmiri, H. Volatile organic compounds removal methods, A review. American Journal of Biochemistry and Biotechnology, 8, 220-229 (2012). https://doi.org/10.3844/ajbbsp.2012.220.229

Brackmann, R., Perez, C.A., Schmal, M., $LaCoO_3$ perovskite on ceramic monoliths- Pre and post reaction analyzes of the partial oxidation of methane. International Journal of Hydrogen Energy, 39, 13991-14007 (2014). https://doi.org/10.1016/j.ijhydene.2014.07.027

Briand, L.E., Jehng, J.-M., Cornaglia, L., Hirt, A.M., Wachs, I.E. Quantitative determination of the number of surface active sites and turnover frequency for methanol oxidation over bulk metal vanadates. Catalysis Today, 78, 257-268 (2003). https://doi.org/10.1016/S0920-5861(02)00350-4

Centeno, M.A., Paulis, M., Montes, M., Odriozola, J.A. Catalytic combustion of volatile organic compounds on Au/CeO2/Al2O3 and Au/Al2O3 catalysts. Applied Catalysis. A: General, 234, 65-78 (2002). https://doi.org/10.1016/S0926-860X(02)00214-4

Chen, W., Tao, X., Zhang, J., Fang, Q., Yang, J. Sol-gel-processed SiO_2/TiO_2/Methylcellulose composite materials for optical waveguides. Journal of the American Ceramic Society, 88, 2998-3002 (2005). https://doi.org/10.1111/j.1551-2916.2005.00543.x

Corma, A., Mocholi, F.A. New silica-alumina-magnesia FCC active matrix and its possibilities as a basic nitrogen passivating compound. Applied Catalysis A: General, 84, 31-46 (1992). https://doi.org/10.1016/0926-860X(92)80337-C

Dai, X.-Y., Shen, F., Ji, J.-Y., Wang, S.-L., Xu, M. Study on extrusion process of SiC ceramic matrix. Materials Science and Engineering, 265, 1-4 (2017). https://doi.org/10.1088/1757-899X/265/1/012031

Dhiman, R., Johnson, E., Skou, E.M., Morgen, P., Andersen, S.M. SiC nanocrystals as Pt catalyst supports for fuel cell applications. Journal of Materials Chemistry A, 1, 6030-6036 (2013). https://doi.org/10.1039/C3TA10238F

Kamitakahara, H., Yoshinaga, A., Aono, H., Nakatsubo, F., Klemm, D., Burchard, W. New approach to unravel the structure- property relationship of methylcellulose. Cellulose, 15, 797-801 (2008). https://doi.org/10.1007/s10570-008-9232-6

Khan, F.I., Ghoshal, A.K. Removal of volatile organic compounds from polluted air. Journal of Loss Prevention in the Process Industries, 13, 527-545 (2000). https://doi.org/10.1016/S0950-4230(00)00007-3

Leclerq, J., Giraud, F., Bianchi, D., Fiaty, K., Gaillard, F. New catalytic system for oxidation of isopropyl alcohol with thin film catalysts. Catalysis Communications, 46, 192-196 (2014). https://doi.org/10.1016/j.catcom.2013.12.022

Ledoux, M.J., Pham-Huu, C. Silicon carbide: A novel catalyst support for heterogeneous catalysis. CAT-TECH, 5, 226-246 (2001). https://doi.org/10.1023/A:1014092930183

Liang, B., Duan, H., Su, X., Chen, X., Huang, Y., Chen, X., Delgado, J.J., Zhang, T. Promoting role of potassium in the reverse water gas shift reaction on Pt/mullite catalyst. Catalysis Today, 281, 319-326 (2017). https://doi.org/10.1016/j.cattod.2016.02.051

Liotta, L.F. Catalytic oxidation of volatile organic compounds on supported noble metals. Applied Catalysis B: Environmental, 100, 403-412 (2010). https://doi.org/10.1016/j.apcatb.2010.08.023

Liu, H., Li, C, Ren, X., Liu, K., Yang, J. Fine platinum nanoparticles supported on a porous ceramic membrane as efficient catalysts for the removal of benzene. Scientific Reports, 7, 1-8 (2017). https://doi.org/10.1038/s41598-017-16833-0

Mizuno, M. Microstructure, microchemistry, and flexural strength of mullite ceramics. Journal of American Ceramic Society, 74, 3017-3022 (1991). https://doi.org/10.1111/j.1151-2916.1991.tb04295.x

Nagai, Y., Dohmae, K., Ikeda, Y., Takagi, N., Hara, N., Tanabe, T., Guilera, G., Pascarelli, S., Newton, M.A., Takahashi, N., Shinjoh, H., Matsumoto, S. In situ observation of platinum sintering on ceria-based oxide for autoexhaust catalysts using Turbo-Xas. Catalysis Today, 175, 133-140 (2011). https://doi.org/10.1016/j.cattod.2011.02.046

Nguyen, N., Edouard, D., Nhut, J.M., Ledoux, M.J., Pham, C., Pham-Huu, C., High thermal conductive β-SiC for selective oxidation of H_2S: A new support for exothermal reactions. Applied Catalysis B: Environmental, 76, 300-310 (2007). https://doi.org/10.1016/j.apcatb.2007.06.007

Orrego-Romero, A.F., Arbelaez-Perez, O.F., Bustamante-Londono, F., Holguin, A.L.V., Pelletization of catalysts supported on activated carbon. A case study: Clean synthesis of dimethyl carbonate from methanol and CO_2. Revista Facultad de Ingeneria, 78, 38-47 (2016). https://doi.org/10.17533/udea.redin.n78a05

Ousmane, M., Liotta, L.F., Di Carlo, G., Pantaleo, G., Venezia, A.M., Deganello, G., Retailleau, L., Boreave, A., Giroir-Fendler, A. Supported Au catalysts for low-temperature abatement of propene and toluene, as model VOCs: support effect. Applied Catalysis B: Environmental, 101, 629-637 (2011). https://doi.org/10.1016/j.apcatb.2010.11.004

Pesant, L., Matta, J., Garin, F., Ledoux, M.J., Bernhardt, P., Pham, C., Pham-Huu, C. A high-performance Pt/β-SiC catalyst for catalytic combustion of model carbon particles (CPs). Applied Catalysis A: General, 266, 21-27 (2004). https://doi.org/10.1016/j.apcata.2004.01.033

Rangelova, N., Radev, L., Nenkova, S., Miranda Salvado, I.M., Vas Fernandes, M.H., Herzog, M. Methylcellulose/SiO_2 hybrids: sol-gel preparation and characterization by XRD, FTIR and AFM. Central European Journal of Chemistry, 9, 112-118 (2011). https://doi.org/10.2478/s11532-010-0123-y

Scirè, S., Minico, S., Crisafulli, C., Satriano, C., Pistone, A., Catalytic combustion of volatile organic compounds on gold/cerium oxide catalysts. Applied Catalysis B: Environmental, 40, 43-49 (2003). https://doi.org/10.1016/S0926-3373(02)00127-3

Sedaghat, A., Taheri-Nassaj, E., Soraru, G.D., Ebadzadeh, T. Microstructure development and phase evolution of alumina-mullite nanocomposite. Science of Sintering, 45, 293-303 (2013). https://doi.org/10.2298/SOS1303293S

Shackelford, J., Doremus, R.H. Ceramic and Glass Materials Structure. Structure, properties and processing. Springer, Boston (2008). https://doi.org/10.1007/978-0-387-73362-3

Schneider, H., Schreuer, J., Hildmann, B. Structure and properties of mullite - A review. Journal of the European Ceramic Society, 28, 329-344 (2008). https://doi.org/10.1016/j.jeurceramsoc.2007.03.017

Spivey, J.J. Complete catalytic oxidation of volatile organics, Industrial & Engineering Chemistry Research, 26, 2165-2180 (1987). https://doi.org/10.1021/ie00071a001

Tu, Y.J., Chang, C.-K., You, C.-F. Combustion of isopropyl alcohol using a green manufactured $CuFe_2O_4$. Journal of Hazardous Materials, 229-230, 258-264 (2012). https://doi.org/10.1016/j.jhazmat.2012.05.100

Xingneng, C., Junyu, C., Yue, Z., Mingshu, C., Huilin, W. Effect of dispersion on catalytic performance of supported Pt catalysts for CO oxidation. Chinese Journal of Catalysis, 33, 1901-1905 (2012). https://doi.org/10.1016/S1872-2067(11)60447-6

Xue, L., Xiong, K., Chen, H., Cho, K., Wang, W. Investigation of the hydrothermal aging of an Mn-based mullite SmMn2O5 catalyst of NO oxidation. RSC Advances, 7, 49091-49096 (2017). https://doi.org/10.1039/C7RA09306C

Yee, A., Morisson, S.J., Idriss, H. The reactions of ethanol over M/CeO_2 catalysts: evidence of carbon-carbon bond dissociation at low temperatures over Rh/CeO_2. Catalysis Today, 63, 327-335 (2000). https://doi.org/10.1016/S0920-5861(00)00476-4

Wang, W., McCool, G., Kapur, N., Yuan, G., Chan, B., Nguyen, M., Graham, U.M., Davis, B.H., Jacobs, G., Cho, K., Hao, X. Mixed-phase oxide on Mn-Mullite (Sn,Gd) Mn_2O_5 for NO oxidation in diesel exhaust. Science, 337, 832-835 (2012). https://doi.org/10.1126/science.1225091